

Loss-induced transparency in optomechanics

H. ZHANG,¹ F. SAIF,² Y. JIAO,¹ AND H. JING^{1,*}

¹*School of Physics and Electronics, Hunan Normal University, Changsha 410081, China
Key Laboratory of Low-Dimensional Quantum Structures and Quantum Control of Ministry of Education,
Department of Physics and Synergetic Innovation Center for Quantum Effects and Applications, Hunan
Normal University, Changsha 410081, China*

²*Department of Electronics, Quaid-i-Azam University, 45320 Islamabad, Pakistan
jinghui73@foxmail.com

Abstract: We study optomechanically induced transparency (OMIT) in a compound system consisting of coupled optical resonators and a mechanical mode, focusing on the unconventional role of loss. We find that optical transparency can emerge at the otherwise strongly absorptive regime in the OMIT spectrum, by using an external nanotip to enhance the optical loss. In particular, loss-induced revival of optical transparency and the associated slow-to-fast light switch can be identified in the vicinity of an exceptional point. These results open up a counterintuitive way to engineer micro-mechanical devices with tunable losses for e.g., coherent optical switch and communications.

© 2018 Optical Society of America under the terms of the [OSA Open Access Publishing Agreement](#)

OCIS codes: (000.0000) General; (000.2700) General science.

References and links

1. M. Aspelmeyer, T. J. Kippenberg, and F. Marquardt, "Cavity optomechanics," *Rev. Mod. Phys.* **86**(4), 1391–1452 (2014).
2. M. Metcalfe, "Applications of cavity optomechanics," *App. Phys. Rev.* **1**(3), 031105 (2014).
3. Milestones: Photons, <https://www.nature.com/milestones/milephotons/timeline.html>.
4. T. J. Kippenberg and K. J. Vahala, "Cavity optomechanics: back-action at the mesoscale," *Science* **321**(5893), 1172–1176 (2008).
5. F. Brennecke, S. Ritter, T. Donner, and T. Esslinger, "Cavity optomechanics with a Bose-Einstein condensate," *Science* **322**(5899), 235–238 (2008).
6. R. Dahan, L. L. Martin, and T. Carmon, "Droplet optomechanics," *Optica* **3**(2), 175–178 (2016).
7. P. Rabl, S. J. Kolkowitz, F. H. L. Koppens, J. G. E. Harris, P. Zoller, and M. D. Lukin, "A quantum spin transducer based on nanoelectromechanical resonator arrays," *Nat. Phys.* **6**(8), 602–608 (2010).
8. J. Bochmann, A. Vainsencher, D. D. Awschalom, and A. N. Cleland, "Nanomechanical coupling between microwave and optical photons," *Nat. Phys.* **9**(11), 712–716 (2013).
9. L. Midolo, A. Schliesser, and A. Fiore, "Nano-opto-electro-mechanical systems," *Nat. Nanotechnol.* **13**(1), 11–18 (2018).
10. E. E. Wollman, C. U. Lei, A. J. Weinstein, J. Suh, A. Kronwald, F. Marquardt, A. A. Clerk, and K. C. Schwab, "Quantum squeezing of motion in a mechanical resonator," *Science* **349**(6251), 952–955 (2015).
11. I. S. Grudinin, H. Lee, O. Painter and K. J. Vahala, "Phonon laser action in a tunable two-level system," *Phys. Rev. Lett.* **104**(8), 083901 (2010).
12. H. Jing, Ş. K. Özdemir, X. Y. Lü, J. Zhang, L. Yang, and F. Nori, " \mathcal{PT} -symmetric phonon laser," *Phys. Rev. Lett.* **113**(5), 053604 (2014).
13. H. Lü, Ş. K. Özdemir, L. M. Kuang, F. Nori, and H. Jing, "Exceptional points in random-defect phonon lasers," *Phys. Rev. Appl.* **8**(4), 044020 (2017).
14. A. G. Krause, M. Winger, T. D. Blasius, Q. Lin, and O. Painter, "A high-resolution microchip optomechanical accelerometer," *Nat. Photonics* **6**(11), 768–772 (2012).
15. E. Gavartin, P. Verlot, and T. J. Kippenberg, "A hybrid on-chip optomechanical transducer for ultrasensitive force measurements," *Nat. Nanotechnol.* **7**(8), 509–514 (2012).
16. G. S. Agarwal and S. Huang, "Electromagnetically induced transparency in mechanical effects of light," *Phys. Rev. A* **81**(4), 041803 (2010).
17. Y.-C. Liu, B.-B. Li, and Y.-F. Xiao, "Electromagnetically induced transparency in optical microcavities," *Nanophotonics* **6**(5), 789–811 (2017).
18. S. Weis, R. Rivière, S. Deléglise, E. Gavartin, O. Arcizet, A. Schliesser, and T. J. Kippenberg, "Optomechanically induced transparency," *Science* **330**(6010), 1520–1523 (2010).

19. A. H. Safavi-Naeini, T. P. Mayer Alegre, J. Chan, M. Eichenfield, M. Winger, Q. Lin, J. T. Hill, D. E. Chang, and O. Painter, "Electromagnetically induced transparency and slow light with optomechanics," *Nature* **472**(7341), 69–73 (2011).
20. J. D. Teufel, D. Li, M. S. Allman, K. Cicak, A. J. Sirois, J. D. Whittaker, and R. W. Simmonds, "Circuit cavity electromechanics in the strong-coupling regime," *Nature* **471**(7337), 204–208 (2011).
21. M. Karuza, C. Biancofiore, M. Bawaj, C. Molinelli, M. Galassi, R. Natali, P. Tombesi, G. Di Giuseppe, and D. Vitali, "Optomechanically induced transparency in a membrane-in-the-middle setup at room temperature," *Phys. Rev. A* **88**(1), 013804 (2013).
22. L. Fan, K. Y. Fong, M. Poot, and H. X. Tang, "Cascaded optical transparency in multimode-cavity optomechanical systems," *Nat. Commun.* **6**, 5850 (2015).
23. C. Dong, J. Zhang, V. Fiore, and H. Wang, "Optomechanically induced transparency and self-induced oscillations with Bogoliubov mechanical modes," *Optica* **1**(6), 425–428 (2014).
24. Z. Shen, C.-H. Dong, Y. Chen, Y.-F. Xiao, F.-W. Sun, and G.-C. Guo, "Compensation of the Kerr effect for transient optomechanically induced transparency in a silica microsphere," *Opt. Lett.* **41**(6), 1249–1252 (2016).
25. K. J. Boller, A. Imamoglu, and S. E. Harris, "Observation of electromagnetically induced transparency," *Phys. Rev. Lett.* **66**(20), 2593 (1991).
26. M. O. Scully and M. S. Zubairy, "Quantum optics," Cambridge University Press, Cambridge, UK (1997).
27. A. Kronwald, and F. Marquardt, "Optomechanically induced transparency in the nonlinear quantum regime," *Phys. Rev. Lett.* **111**(13), 133601 (2013).
28. H. Xiong, L.-G. Si, A.-S. Zheng, X. Yang, and Y. Wu, "Higher-order sidebands in optomechanically induced transparency," *Phys. Rev. A* **86**(1), 013815 (2012).
29. Y. Jiao, H. Lü, J. Qian, Y. Li, and H. Jing, "Nonlinear optomechanics with gain and loss: amplifying higher-order sideband and group delay," *New J. Phys.* **18**, 083034 (2016).
30. Y. F. Jiao, T. X. Lu, and H. Jing, "Optomechanical second-order sidebands and group delays in a Kerr resonator," *Phys. Rev. A* **97**(1), 013843 (2018).
31. H. Wang, X. Gu, Y. Liu, A. Miranowicz, and F. Nori, "Optomechanical analog of two-color electromagnetically induced transparency: Photon transmission through an optomechanical device with a two-level system," *Phys. Rev. A* **90**(2), 023817 (2014).
32. K. Ullah, H. Jing, and F. Saif, "Multiple electromechanically-induced-transparency windows and Fano resonances in hybrid nano-electro-optomechanics," *Phys. Rev. A* **97**(3), 033812 (2018).
33. H. Lü, Y. Jiang, Y. Z. Wang, and H. Jing, "Optomechanically induced transparency in a spinning resonator," *Photonics Res.* **5**(4), 367–371 (2017).
34. H. Jing, Ş. K. Özdemir, Z. Geng, J. Zhang, X. Y. Lü, B. Peng, L. Yang, and F. Nori, "Optomechanically-induced transparency in parity-time-symmetric microresonators," *Sci. Rep.* **5**, 9663 (2015).
35. V. Fiore, C. Dong, M. C. Kuzyk, and H. Wang, "Optomechanical light storage in a silica microresonator," *Phys. Rev. A* **87**(2), 023812 (2013).
36. Y. Guo, K. Li, W. Nie, and Y. Li, "Electromagnetically-induced-transparency-like ground-state cooling in a double-cavity optomechanical system," *Phys. Rev. A* **90**(5), 053841 (2014).
37. T. Ojanen and K. Børkje, "Ground-state cooling of mechanical motion in the unresolved sideband regime by use of optomechanically induced transparency," *Phys. Rev. A* **90**(1), 013824 (2014).
38. Y.-C. Liu, Y.-F. Xiao, X.-S. Luan, and W. C. Wei, "Optomechanically-induced-transparency cooling of massive mechanical resonators to the quantum ground state," *Sci. China-Phys. Mech. Astron.* **58**(5), 050305 (2015).
39. J. Q. Zhang, Y. Li, M. Feng, and Y. Xu, "Precision measurement of electrical charge with optomechanically induced transparency," *Phys. Rev. A* **86**(5), 053806 (2012).
40. H. Xiong, L.-G. Si, and Y. Wu, "Precision measurement of electrical charges in an optomechanical system beyond linearized dynamics," *Appl. Phys. Lett.* **110**(17), 171102 (2017).
41. J. Fan, and L. Zhu, "Enhanced optomechanical interaction in coupled microresonators," *Opt. Express* **20**(18), 20790 (2012).
42. X.-W. Xu and Y.-J. Li, "Antibunching photons in a cavity coupled to an optomechanical system," *J. Phys. B: At. Mol. Opt. Phys.* **46**(3), 035502 (2013).
43. G. Li, X. Jiang, S. Hua, Y. Qin, and M. Xiao, "Optomechanically tuned electromagnetically induced transparency-like effect in coupled optical microcavities," *Appl. Phys. Lett.* **109**(26), 261106 (2016).
44. B. Peng, Ş. K. Özdemir, F. Lei, F. Monifi, M. Gianfreda, G. L. Long, S. Fan, F. Nori, C. M. Bender, and L. Yang, "Parity-time-symmetric whispering-gallery microcavities," *Nat. Phys.* **10**(5), 394–398 (2014).
45. L. Chang, X. Jiang, S. Hua, C. Yang, J. Wen, L. Jiang, G. Li, G. Wang, and M. Xiao, "Parity-time symmetry and variable optical isolation in active-passive-coupled microresonators," *Nat. Photonics* **8**(7), 524–529 (2014).
46. X.-Y. Lü, H. Jing, J.-Y. Ma, and Y. Wu, " \mathcal{PT} -symmetry-breaking chaos in optomechanics," *Phys. Rev. Lett.* **114**(25), 253601 (2015).
47. H. Xu, D. Mason, L. Jiang, and J. G. E. Harris, "Topological energy transfer in an optomechanical system with exceptional points," *Nature* **537**(7618), 80–83 (2016).
48. H. Jing, Ş. K. Özdemir, H. Lü, and F. Nori, "High-order exceptional points in optomechanics," *Sci. Rep.* **7**, 3386 (2017).
49. C. M. Bender and S. Boettcher, "Real spectra in non-Hermitian Hamiltonians having \mathcal{PT} symmetry," *Phys. Rev.*

- Lett. **80**(24), 5243–5246 (1998).
50. C. M. Bender, "Making sense of non-Hermitian Hamiltonians," *Rep. Prog. Phys.* **70**(6), 947–1018 (2007).
 51. C. M. Bender, M. Gianfreda, Ş. K. Özdemir, B. Peng, and L. Yang, "Twofold transition in \mathcal{PT} -symmetric coupled oscillators," *Phys. Rev. A* **88**(6), 062111 (2013).
 52. V. V. Konotop, J. Yang, and D. A. Zezyulin, "Nonlinear waves in \mathcal{PT} -symmetric systems," *Rev. Mod. Phys.* **88**(3), 035002 (2016).
 53. R. El-Ganainy, K. G. Makris, M. Khajavikhan, Z. H. Musslimani, S. Rotter, and D. N. Christodoulides, "Non-Hermitian physics and \mathcal{PT} symmetry," *Nat. Phys.* **14**(1), 11–19 (2018).
 54. L. Feng, R. El-Ganainy, and L. Ge, "Non-Hermitian photonics based on parity-time symmetry," *Nat. Photonics* **11**(12), 752–762 (2017).
 55. B. Peng, Ş. K. Özdemir, S. Rotter, H. Yilmaz, M. Liertzer, F. Monifi, C. M. Bender, F. Nori, and L. Yang, "Loss-induced suppression and revival of lasing," *Science* **346**(6207), 328–332 (2014).
 56. A. Guo, G. J. Salamo, D. Duchesne, R. Morandotti, M. Volatier-Ravat, V. Aimez, G. A. Siviloglou, and D. N. Christodoulides, "Observation of \mathcal{PT} -symmetry breaking in complex optical potentials," *Phys. Rev. Lett.* **103**(9), 093902 (2009).
 57. J. Zhu, Ş. K. Özdemir, L. He, and L. Yang, "Controlled manipulation of mode splitting in an optical microcavity by two Rayleigh scatterers," *Opt. Express* **18**(23), 23535–23543 (2010).
 58. C. W. Gardiner and M. J. Collett, "Input and output in damped quantum systems: Quantum stochastic differential equations and the master equation," *Phys. Rev. A* **31**(6), 3761–3774 (1985).
 59. T. Oishi and M. Tomita, "Inverted coupled-resonator-induced transparency," *Phys. Rev. A* **88**(1), 013813 (2013).
 60. A. A. Zyblovsky, A. P. Vinogradov, A. A. Pukhov, A. V. Dorofeenko, and A. A. Lisyansky, " \mathcal{PT} -symmetry in optics," *Phys. Usp.* **57**(11), 1063–1082 (2014).
 61. H. Hodaei, A. U. Hassan, S. Wittek, H. Garcia-Gracia, R. El-Ganainy, D. N. Christodoulides, and M. Khajavikhan, "Enhanced sensitivity at higher-order exceptional points," *Nature* **548**(7666), 187–191 (2017).
 62. W. Chen, Ş. K. Özdemir, G. Zhao, J. Wiersig, and L. Yang, "Exceptional points enhance sensing in an optical microcavity," *Nature* **548**(7666), 192–196 (2017).
 63. A. U. Hassan, H. Hodaei, D. N. Christodoulides and M. Khajavikhan, "Exceptional points: an emerging tool for sensor applications," *Optics & Photonics News*, **2018**(01), 20–22 (2018).
 64. D. A. Zezyulin and V. V. Konotop, "Nonlinear modes in finite-dimensional \mathcal{PT} -symmetric systems," *Phys. Rev. Lett.* **108**(21), 213906 (2012).
-

1. Introduction

Cavity optomechanics (COM) [1, 2], viewed as a new milestone [3] in the history of optics, has significantly extended fundamental studies and practical applications of coherent light-matter interactions. A wide range of COM devices, such as solid-state resonators [4], atomic gases [5], or liquid droplets [6], has been created for diverse purposes. Important applications of these devices [2] include quantum transducer [7–9], mechanical squeezing [10], phonon lasing [11–13], and ultra-sensitive motion sensing [14, 15]. Another intriguing example closely related to the present work is optomechanically induced transparency (OMIT) [16–24], as already demonstrated in e.g., a microtoroid resonator [18], a crystal-nanobeam system [19], a microwave circuit [20], a membrane-in-the-middle cavity [21], a cascaded COM device [22], an optical cavity coupled to Bogoliubov mechanical modes [23], and a nonlinear Kerr resonator [24]. OMIT is generally viewed as an analog of electromagnetically induced transparency (EIT) well-known in atomic physics [25, 26], i.e., arising due to destructive interference of two absorption channels of the probe photons (by the cavity or the phonon mode). Beyond this picture, novel effects have also been revealed, such as nonlinear OMIT [27–30], two-color OMIT [31, 32], nonreciprocal OMIT [33], and reversed OMIT [34]. Promising applications of OMIT devices are actively explored as well, such as optical memory [19, 35], phononic engineering [36–38], and precision measurements [39, 40].

In this work, we study the unexpected role of loss in OMIT with a compound COM system. We note that in comparison with single-cavity devices, coupled-cavity COM has several unique properties enabling more advantages in applications. For example, both the input light and its frequency sideband can be resonantly tuned to achieve efficient phonon cooling [41]. The inter-cavity coupling strength, strongly affecting the circulating power in the resonators, also provides a tunable parameter to realize e.g., phonon lasing [11–13], unconventional photon

blockade [42], reversed OMIT [34], and highly-efficient optical control [43]. In particular, by coupling an active (e.g., Erbium ion-doped) resonator to a lossy one [44, 45], COM devices with an exceptional point (EP) [12, 13, 34, 46–48], featuring non-Hermitian coalescence of both eigenvalues and eigenfunctions [49–51], can be created. In view of novel functionalities enabled by EP devices, e.g., single-mode lasing or ultrahigh-sensitive sensing [52–54], this opens up a new route to operate COM devices at EPs for various applications.

Here we probe the EP features in OMIT, without using any active gain, but increasing the optical loss [55, 56]. We note that in a recent experiment [55], by placing an external nanotip near a microresonator and thus increasing the optical loss, counterintuitive EP features, i.e., suppression and revival of lasing were demonstrated [55]. Similar EP features in optical transmissions, i.e., loss-induced transparency (LIT) were reported previously in a purely optical experiment [56]. Our purpose here is to show the LIT features in OMIT devices, i.e., loss-induced suppression and revival of optical transparency at the EP. In addition, we find that by increasing the optical loss, strong absorption regimes in conventional OMIT can become transparent, accompanying by a slow-to-fast light switch in the vicinity of the EP (for similar reversed-OMIT features, see also Ref. [34] in an active COM system). The unconventional role of loss on the higher-order OMIT sidebands [28–30] is also probed. These results indicate a counterintuitive way to achieve optical switch and communications with OMIT devices, without the need of any active gain or complicated materials.

2. Model and results

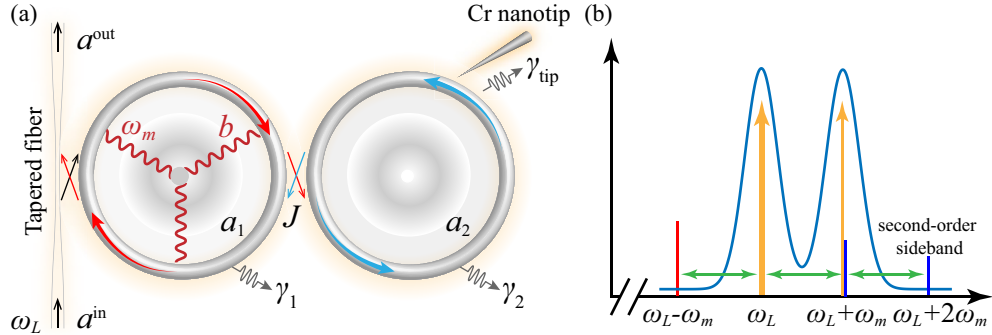


Fig. 1. (a) Schematic diagram of the compound COM system, with an additional optical loss γ_{tip} induced by a Cr-coated nanofiber tip on the right (i.e., purely optical) resonator [55, 56]. (b) The frequency spectrum of the compound COM system, with the red line or the blue lines denoting the red sideband (Stokes process) or the blue sidebands (anti-Stokes process), respectively [18, 19].

As shown in Fig. 1, we consider two whispering-gallery-mode (WGM) microtoroid resonators coupled through evanescent fields, with the tunable coupling strength J and the intrinsic optical loss γ_1 or γ_2 , respectively [44, 55]. The external lights are input and output via tapered-fiber waveguides. As in Refs. [55, 56], an additional optical loss γ_{tip} is induced on the right (i.e., purely optical) resonator by a chromium (Cr)-coated silica nanofiber tip [57], in order to see the loss effects on such a compound COM system. The left resonator, supporting also a mechanical mode of frequency ω_m and an effective mass m , is driven by a strong red-detuned pump laser at frequency ω_L and a weak probe laser at frequency ω_P [18, 19], with the optical field amplitudes

$$\varepsilon_L = \sqrt{2\gamma_c P_L / \hbar\omega_L}, \quad \varepsilon_P = \sqrt{2\gamma_c P_{\text{in}} / \hbar\omega_P}, \quad (1)$$

respectively, where for simplicity we take $\gamma_1 = \gamma_2 = \gamma_c$ and P_L or P_{in} is the power of the pump or the probe light.

In a frame rotating at frequency ω_L , the Hamiltonian of this compound COM system can be written at the simplest level as

$$\begin{aligned} H &= H_0 + H_{\text{int}} + H_{\text{dr}}, \\ H_0 &= \frac{p^2}{2m} + \frac{1}{2}m\omega_m^2 x^2 + \hbar\Delta_L(a_1^\dagger a_1 + a_2^\dagger a_2), \\ H_{\text{int}} &= -\hbar J(a_1^\dagger a_2 + a_2^\dagger a_1) - \hbar g a_1^\dagger a_1 x, \\ H_{\text{dr}} &= i\hbar\varepsilon_L(a_1^\dagger - a_1) + i\hbar\varepsilon_P(a_1^\dagger e^{-i\epsilon t} - a_1 e^{i\epsilon t}), \end{aligned} \quad (2)$$

where ω_c is the resonant frequency of the optical mode, a_1 (a_1^\dagger) and a_2 (a_2^\dagger) are the optical bosonic annihilation (creation) operators, g denotes the COM coupling strength, x or p is the mechanical displacement or momentum operator, and the optical detunings are

$$\Delta_L = \omega_c - \omega_L, \quad \epsilon = \omega_P - \omega_L. \quad (3)$$

The Heisenberg equations of motion of this compound system are

$$\begin{aligned} \ddot{x} &= -\Gamma_m \dot{x} - \omega_m^2 x + \frac{\hbar g}{m} a_1^\dagger a_1, \\ \dot{a}_1 &= (-i\Delta_L - \gamma_1 + igx)a_1 + iJ a_2 + \varepsilon_L + \varepsilon_P e^{-i\epsilon t}, \\ \dot{a}_2 &= (-i\Delta_L - \gamma_2 - \gamma_{\text{tip}})a_2 + iJ a_1, \end{aligned} \quad (4)$$

where Γ_m is the mechanical loss rate. For $\varepsilon_P \ll \varepsilon_L$, we can take the probe light as a perturbation, the dynamical variables can be expressed as $a_i = a_{i,s} + \delta a_i$ ($i=1,2$) and $x = x_s + \delta x$, where the steady-state solutions of the system, by setting all the derivatives of the variables as zero, are easily obtained as

$$\begin{aligned} x_s &= \frac{\hbar g}{m\omega_m^2} |a_{1,s}|^2, \\ a_{1,s} &= \frac{\varepsilon_L (i\Delta_L + \gamma_2 + \gamma_{\text{tip}})}{(i\Delta_L + \gamma_1 - igx_s) (i\Delta_L + \gamma_2 + \gamma_{\text{tip}}) + J^2}, \\ a_{2,s} &= \frac{iJ\varepsilon_L}{(i\Delta_L + \gamma_1 - igx_s) (i\Delta_L + \gamma_2 + \gamma_{\text{tip}}) + J^2}. \end{aligned} \quad (5)$$

For comparisons, we first consider the purely optical case [56] by ignoring the COM coupling. In this special case, by using the input-output relation [58] $a_1^{\text{out}} = a_1^{\text{in}} - \sqrt{2\gamma_1} a_1$, we can derive the optical transmission rate as

$$T = \left| \frac{a_1^{\text{out}}}{a_1^{\text{in}}} \right|^2 = \left| 1 - \frac{2\gamma_1 (i\Delta_2 + \gamma_2 + \gamma_{\text{tip}})}{(i\Delta_1 + \gamma_1) (i\Delta_2 + \gamma_2 + \gamma_{\text{tip}}) + J^2} \right|^2, \quad (6)$$

where $\Delta_i = \omega_P - \omega_i$ ($i = 1, 2$) is the detuning between the probe and the cavity mode. For simplicity, here we take $\Delta_1 = \Delta_2 = \Delta_P$. As shown in Fig. 2(a), the LIT feature can be clearly seen at the resonance (i.e., $\Delta_P = 0$) in the transmission spectrum, that is, the transmission rate firstly decreases and then increases by increasing the tip loss γ_{tip} [56]. The turning point (TP) position turns out to be

$$\gamma_{\text{tip}}^{\text{TP}} = -(i\Delta_2 + \gamma_2) + \frac{(i\Delta_1 + \gamma_1)J^2}{\Delta_1^2 + \gamma_1^2}, \quad (7)$$

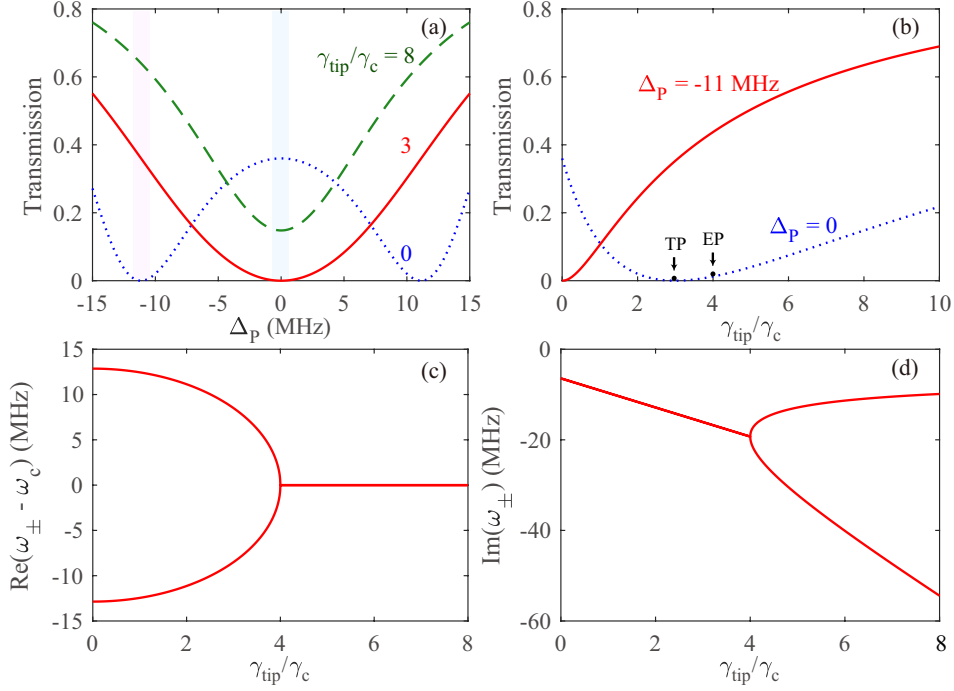


Fig. 2. (a) Transmission rate of the coupled optical system as a function of Δ_p at three selected $\gamma_{\text{tip}}/\gamma_c$. (b) Transmission rate as a function of γ_{tip} when Δ_p is 0 and -11 MHz. Evolution of the real (c) and imaginary (d) parts of the eigenfrequencies of the supermodes as a function of the loss γ_{tip} . The parameters used here are $\gamma_1 = \gamma_2 = \gamma_c = 6.43$ MHz and $J/\gamma_c = 2$.

which, for the parameter values chosen here, corresponds to $\gamma_{\text{tip}}^{\text{TP}}/\gamma_c = 3$ (illustrated in Fig. 2(b)). Interestingly, we also note that by increasing γ_{tip} , the strong-absorption regimes in the conventional transmission spectrum (at $\Delta_p = \pm 11$ MHz) become transparent, see Fig. 2(b), which is not reported in Ref. [56]. This phenomenon is induced by the reduction of interference caused by the tip loss. And from our numerical estimation, $\gamma_{\text{tip}}^{\text{TP}}$ is ~ 0 for $\Delta_p = \pm 11$ MHz, i.e., by reversing the tip loss to an active gain, it is possible to reverse the dip in the EIT spectrum to a peak as already observed in the recent reversed EIT experiment performed by T. Oishi and M. Tomita [59]. LIT is generally viewed as the evidence of the EP emergence in this lossy system [56], or the existence of hidden parity-time symmetry (under a suitable mathematical transformation) [60]. The eigenfrequencies of this coupled optical system are

$$\omega_{\pm} = \frac{1}{2} [(\omega_1 + \omega_2) - i(\gamma_1 + \gamma_2 + \gamma_{\text{tip}})] \pm \frac{1}{2} \sqrt{[(\omega_1 - \omega_2) + i(\gamma_2 + \gamma_{\text{tip}} - \gamma_1)]^2 + 4J^2}. \quad (8)$$

For $\omega_1 = \omega_2 = \omega_c$, the EP condition is simplified as $\gamma_{\text{tip}}^{\text{EP}} = \gamma_1 - \gamma_2 + 2J$, or for the parameter values chosen here, $\gamma_{\text{tip}}^{\text{EP}}/\gamma_c = 4$, see Fig. 2(c-d). Clearly, $\gamma_{\text{tip}}^{\text{TP}}$ can be close to but not exactly coincides with $\gamma_{\text{tip}}^{\text{EP}}$, due to the fact that the TP depends on the detuning $\Delta_{1,2}$ while the EP does not (for similar features, see also Ref. [55]).

Now we consider the role of COM coupling in LIT. For this aim, we express the dynamical variables as the sum of their steady-state values and small fluctuations to the first order, i.e.,

$$x = x_s + \delta x^{(1)} + \dots, \quad a_i = a_{i,s} + \delta a_i^{(1)} + \dots \quad (i = 1, 2), \quad (9)$$

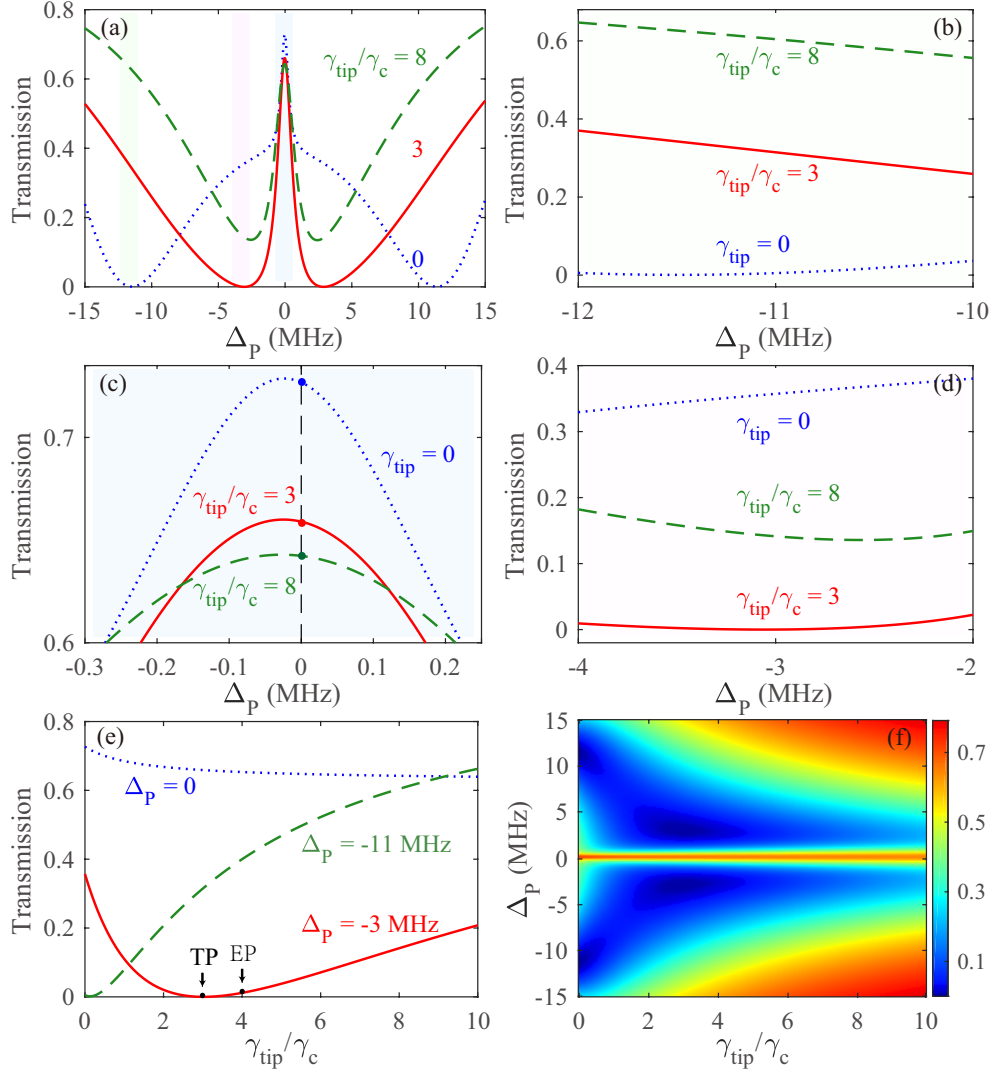


Fig. 3. (a)–(d) Transmission rate T_P of the probe light as a function of Δ_p . (e) Transmission rate of OMIT as a function of γ_{tip} at different Δ_p . (f) Transmission rate of OMIT as a function of γ_{tip} and Δ_p . The other parameters are $\omega_c = 193$ THz, $\gamma_c = 6.43$ MHz, $\omega_m = 2\pi \times 23.4$ MHz, $P_L = 1$ mW, $\Delta_L = \omega_m$, $g = \omega_c/R$, $R = 34.5$ μm , $m = 5 \times 10^{-11}$ kg, $J = 12.86$ MHz and $\Gamma_m = 0.24$ MHz.

with which we can rewrite the equations of motion as

$$\begin{aligned}
 \frac{d^2}{dt^2}(x_s + \delta x^{(1)}) &= -\Gamma_m \frac{d}{dt}(x_s + \delta x^{(1)}) - \omega_m^2(x_s + \delta x^{(1)}) + \frac{\hbar g}{m}(a_{1,s} + \delta a_1^{(1)})(a_{1,s} + \delta a_1^{(1)}), \\
 \frac{d}{dt}(a_{1,s} + \delta a_1^{(1)}) &= [-i\Delta_L - \gamma_1 + ig(x_s + \delta x^{(1)})](a_{1,s} + \delta a_1^{(1)}) + iJ(a_{2,s} + \delta a_2^{(1)}) \\
 &\quad + \varepsilon_L + \varepsilon_P e^{-i\epsilon t}, \\
 \frac{d}{dt}(a_{2,s} + \delta a_2^{(1)}) &= (-i\Delta_L - \gamma_2 - \gamma_{\text{tip}})(a_{2,s} + \delta a_2^{(1)}) + iJ(a_{1,s} + \delta a_1^{(1)}).
 \end{aligned} \tag{10}$$

Here the higher-order terms such as $\delta x^{(1)}\delta a_1^{(1)}$ will be neglected since they only contribute to the higher-order sidebands [28].

Then by using the ansatz:

$$\begin{pmatrix} \delta a_i^{(1)} \\ \delta x^{(1)} \end{pmatrix} = \begin{pmatrix} \delta a_{i+}^{(1)} \\ \delta x_+^{(1)} \end{pmatrix} e^{-i\epsilon t} + \begin{pmatrix} \delta a_{i-}^{(1)} \\ \delta x_-^{(1)} \end{pmatrix} e^{i\epsilon t} \quad (i = 1, 2), \quad (11)$$

we obtain the solutions for the fluctuation operators as

$$\delta x_+^{(1)} = \frac{\hbar g \epsilon_P a_{1,s}^* \mu_-^{(1)} \mathcal{A}_1^{(1)}}{\mathcal{K}^{(1)} \mathcal{A}_1^{(1)} \mathcal{A}_2^{(1)} + i \hbar g^2 |a_{1,s}|^2 (\mu_+^{(1)*} \mathcal{A}_2^{(1)} - \mu_-^{(1)} \mathcal{A}_1^{(1)})}, \quad (12)$$

$$\delta a_{1+}^{(1)} = \frac{\epsilon_P \mu_-^{(1)} (\mathcal{K}^{(1)} \mathcal{A}_1^{(1)} + i \hbar g^2 |a_{1,s}|^2 \mu_+^{(1)*})}{\mathcal{K}^{(1)} \mathcal{A}_1^{(1)} \mathcal{A}_2^{(1)} + i \hbar g^2 |a_{1,s}|^2 (\mu_+^{(1)*} \mathcal{A}_2^{(1)} - \mu_-^{(1)} \mathcal{A}_1^{(1)})}, \quad (13)$$

where $\mathcal{K}^{(1)} = m(-\epsilon^2 - i\epsilon\Gamma_m + \omega_m^2)$ and

$$\begin{aligned} \mathcal{A}_1^{(1)} &= \mu_+^{(1)*} \nu_+^{(1)*} + J^2, & \mathcal{A}_2^{(1)} &= \mu_-^{(1)} \nu_-^{(1)} + J^2, \\ \mu_{\pm}^{(1)} &= i\Delta_L + \gamma_2 + \gamma_{\text{tip}} \pm i\epsilon, & \nu_{\pm}^{(1)} &= i\Delta_L + \gamma_1 - igx_s \pm i\epsilon. \end{aligned} \quad (14)$$

With these results at hand, by using the standard input-output relation [58], we can obtain the transmission rate of the probe light

$$T_P = \left| \frac{a_1^{\text{out}}}{a_1^{\text{in}}} \right|^2 = \left| \frac{\epsilon_P - 2\gamma_1 \delta a_{1+}^{(1)}}{\epsilon_P} \right|^2 = \left| 1 - \frac{2\gamma_1 \delta a_{1+}^{(1)}}{\epsilon_P} \right|^2, \quad (15)$$

which describes the relation of the output field amplitude and the input field amplitude at the probe frequency.

Figure 3 shows the transmission rate T_P of the probe as a function of Δ_P and γ_{tip} . We see that (i) the strong-absorption regimes at $\Delta_P = \pm 11$ MHz become transparent by increasing the tip loss, e.g., T_P is increased from zero to ~ 0.35 or ~ 0.6 for $\gamma_{\text{tip}}/\gamma_c \sim 3$ or 8, see Fig. 3(b) which is same as the purely optical case. In contrast, (ii) for the resonant case ($\Delta_P = 0$), the OMIT peak tends to be lowered, i.e., T_P decreases for more tip loss, with its linewidth firstly decreased but then increased again, see Fig. 3(a,c). More interestingly, (iii) for the intermediate regime ($\Delta_P = \pm 3$ MHz), the feature as LIT in purely optical systems [55, 56] in the resonant case can be clearly seen, i.e., T_P firstly drops down to zero but then increases again for more tip loss, with the turning point $\gamma_{\text{tip}}^{\text{TP}}/\gamma_c = 3$, see Fig. 3(d). A more intuitive analysis of these phenomena in the various parametric regimes is shown in Fig. 3(e) and the TP and EP are illustrated in the figure. In Fig. 3(f), the transmission rate is plotted as a function of γ_{tip} and Δ_P which are both continuously varying to give a comprehensive view.

Based on the analyses above, we find that the LIT emerging at the resonance in the purely optical system now moves to the off-resonance regime of a specific detuning ($\Delta_P = \pm 3$ MHz) in the COM system. We will give an analysis of this difference in the following section. By comparing the linearized equations of $\delta a_{1+}^{(1)}$ corresponding to the optical case and the COM case

$$(i\Delta_L + \gamma_1 - i\epsilon) \delta a_{1+}^{(1)} = iJ\delta a_{2+}^{(1)} + \epsilon_P, \quad (16)$$

$$(i\Delta_L + \gamma_1 - igx_s - i\epsilon) \delta a_{1+}^{(1)} = ig a_{1,s} \delta x_+^{(1)} + iJ\delta a_{2+}^{(1)} + \epsilon_P, \quad (17)$$

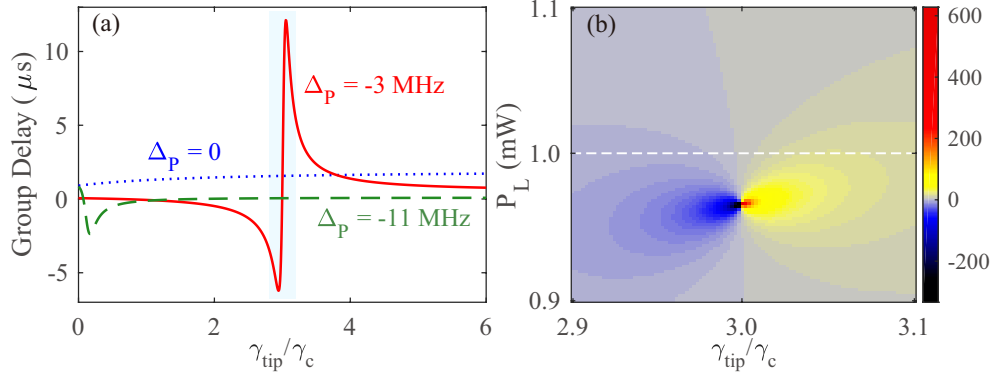


Fig. 4. (a) Group delay of the probe light as a function of γ_{tip} at different Δ_p . The pump power P_L is 1 mW. (b) Group delay of the probe light as a function of γ_{tip} and the pump power P_L at $\Delta_p = -3$ MHz. The unit of group delay is μs .

we can see that the differences are the COM terms: $-igx_s\delta a_{1+}^{(1)}$, $iga_{1,s}\delta x_+^{(1)}$. Then we transform Eq. (17) into a form similar to Eq. (16) utilizing the linearized equation of $\delta x_+^{(1)}$

$$(i\Delta' + \gamma_1' - i\epsilon)\delta a_{1+}^{(1)} = iJ\delta a_{2+}^{(1)} + \epsilon_P, \quad (18)$$

where

$$\Delta' = \Delta_L - gx_s - \text{Re}(C_1), \quad \gamma_1' = \gamma_1 + \text{Im}(C_1), \quad (19)$$

and

$$C_1 = \frac{\mathcal{A}_1^{(1)}\hbar g^2 |a_{1,s}|^2}{\mathcal{A}_1^{(1)}\mathcal{K}^{(1)} + i\hbar g^2 |a_{1,s}|^2 (-i\Delta_L + \gamma_2 + \gamma_{\text{tip}} - i\epsilon)}. \quad (20)$$

With chosen parameters above, we can numerically estimate a frequency shift of $gx_s + \text{Re}(C_1)$ to be ~ 3 MHz in the steady-state case. For comparison with purely optical system, we choose $\Delta_L = 0$ and $\Delta_p = 0$. This frequency shift caused by the COM interaction is matched well with the parametric regimes where we find the LIT at the detuning of $\Delta_p = \pm 3$ MHz in the transmission spectrum of OMIT.

Now we turn to the slow-to-fast-light switch at the EP. Slowing or advancing of light can be associated with the OMIT process due to the abnormal dispersion [19]. This feature can be characterized by the group delay of the probe light

$$\tau_g = \frac{d \arg(T_P)}{d \Delta_p}, \quad (21)$$

Figure 4 shows the group delay as a function of γ_{tip} at different values of Δ_p . We find that at $\Delta_p = -3$ MHz, the probe light experiences a fast-to-slow switch in the vicinity of the EP, a feature which is similar to the reverted OMIT reported previously in an active COM system [34]. This provides a new method to achieve coherent optical group-velocity switch by tuning the optical loss, which as far as we know, has not been demonstrated previously in purely optical systems. In view of the sensitive change of τ_g at the EP, this also could be used for e.g., EP-enhanced sensing of external particles entering into the mode volume of the resonator [61–63].

3. Second-order LIT in COM

In contrast to the linear systems [55, 56], the tip loss can also affect the higher-order process originating from intrinsic nonlinear COM interactions. In order to see this, we use the following

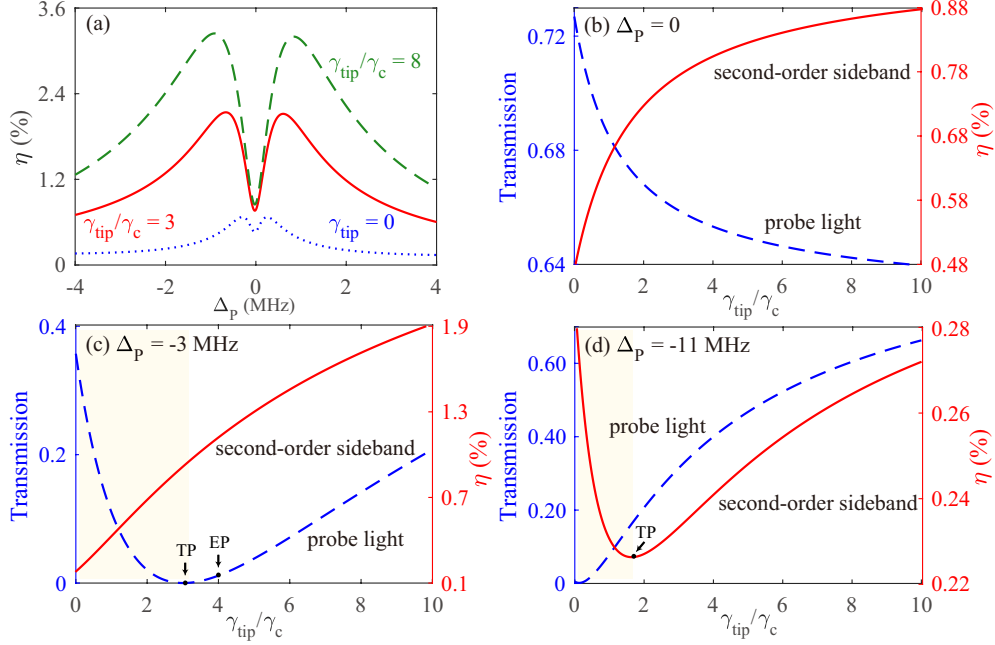


Fig. 5. (a) The efficiency of the second-order sideband process as a function of Δ_p . Subfigures (b), (c) and (d) show the comparisons between transmission rate of OMIT and efficiency of the second-order sideband as a function of γ_{tip} .

second-order expansions of the operators [28]

$$x = x_s + \delta x^{(1)} + \delta x^{(2)} + \dots, \quad a_i = a_{i,s} + \delta a_i^{(1)} + \delta a_i^{(2)} + \dots \quad (i = 1, 2), \quad (22)$$

with

$$\begin{pmatrix} \delta a_i^{(2)} \\ \delta x^{(2)} \end{pmatrix} = \begin{pmatrix} \delta a_{i+}^{(2)} \\ \delta x_+^{(2)} \end{pmatrix} e^{-2i\epsilon t} + \begin{pmatrix} \delta a_{i-}^{(2)} \\ \delta x_-^{(2)} \end{pmatrix} e^{2i\epsilon t} \quad (i = 1, 2). \quad (23)$$

Then by solving the Eq. (4), with the aid of Eqs. (11,22,23) and neglecting the higher-order terms more than second order, we get the second-order solutions

$$\delta a_{1+}^{(2)} = \frac{-i\hbar g^4 a_{1,s} |a_{1,s}|^2 \mu_+^{(1)*} \mu_+^{(2)*} \mu_-^{(2)} \delta x_+^{(1)2} + \lambda \delta x_+^{(1)} \delta a_{1+}^{(1)}}{\mathcal{A}_1^{(1)} \left[\mathcal{K}^{(2)} \mathcal{A}_1^{(2)} \mathcal{A}_2^{(2)} + i\hbar g^2 |a_{1,s}|^2 \left(\mathcal{A}_2^{(2)} \mu_+^{(2)*} - \mathcal{A}_1^{(2)} \mu_-^{(2)} \right) \right]}, \quad (24)$$

with $\mathcal{K}^{(2)} = m(-4\epsilon^2 - 2i\epsilon\Gamma_m + \omega_m^2)$ and

$$\begin{aligned} \mathcal{A}_1^{(2)} &= \mu_+^{(2)*} \nu_+^{(2)*} + J^2, & \mathcal{A}_2^{(2)} &= \mu_-^{(2)} \nu_-^{(2)} + J^2, \\ \mu_{\pm}^{(2)} &= i\Delta_L + \gamma_2 + \gamma_{\text{tip}} \pm 2i\epsilon, & \nu_{\pm}^{(2)} &= i\Delta_L + \gamma_1 - igx_s \pm 2i\epsilon, \\ \lambda &= ig\mu_-^{(2)} \mathcal{K}^{(2)} \mathcal{A}_1^{(1)} \mathcal{A}_1^{(2)} - \hbar g^3 |a_{1,s}|^2 \mu_-^{(2)} \left(\mathcal{A}_1^{(1)} \mu_+^{(2)*} - \mu_+^{(1)*} \mathcal{A}_1^{(2)} \right). \end{aligned} \quad (25)$$

As defined in Ref. [28], the efficiency of the second-order sideband process is

$$\eta = \left| -\frac{2\gamma_1}{\epsilon_P} \delta a_{1+}^{(2)} \right|. \quad (26)$$

Figure 5(a) shows the impact of the tip loss on the second-order sideband of OMIT. We find that, in contrast to the linear cases, the efficiency η increases by enhancing the loss γ_{tip} . A comparison between T_P and η is shown in Fig. 5(b-d). Figure 5(b) shows that T_P decreases by increasing γ_{tip} at the resonance while η is enhanced, a feature which was firstly revealed in Ref. [28]. However, for non-resonance cases, e.g., $\Delta_P = \pm 3$ MHz or $\Delta_P = \pm 11$ MHz, η increases by increasing γ_{tip} , which is evidently different from that for T_P , see Fig. 5(c-d). Clearly, these results on nonlinear OMIT process are beyond any linear EP picture [48]. We note that the presence of nonlinearity can lead to a shift of the EP position [64] or even the emergence of high-order EPs [48]. We also note that η_{TP} emerges at $\Delta_P = \pm 11$ MHz, which is clearly different from the linear TP occurring at $\Delta_P = \pm 3$ MHz. In fact, this frequency shift can also be identified by comparing the equations describing the linear process and its second-order sidebands, i.e.,

$$(i\Delta' + \gamma_1' - i\epsilon) \delta a_{1+}^{(1)} = iJ\delta a_{2+}^{(1)} + \epsilon_P, \quad (27)$$

$$(i\Delta'' + \gamma_1'' - 2i\epsilon) \delta a_{1+}^{(2)} = iJ\delta a_{2+}^{(2)} + \mathcal{B}, \quad (28)$$

with

$$\Delta'' = \Delta_L - gx_s - \mathbf{Re}(C_2), \quad \gamma_1'' = \gamma_1 + \mathbf{Im}(C_2), \quad (29)$$

and

$$C_2 = \frac{\hbar g^2 |a_{1,s}|^2 \mathcal{A}_1^{(2)} \mathcal{A}_1^{(1)}}{\mathcal{A}_1^{(2)} \mathcal{A}_1^{(1)} \mathcal{K}^{(2)} + i\hbar g^2 |a_{1,s}|^2 \mathcal{A}_1^{(1)} \mu_+^{(2)*}}, \quad (30)$$

$$\mathcal{B} = \frac{i\hbar g^2 a_{1,s} \left[-g^2 |a_{1,s}|^2 \mu_+^{(2)*} \mu_+^{(1)*} \delta x_+^{(1)2} - ig \mathcal{A}_1^{(2)} a_{1,s}^* \mu_+^{(1)*} \delta x_+^{(1)} \delta a_{1+}^{(1)} \right]}{\mathcal{A}_1^{(2)} \mathcal{A}_1^{(1)} \mathcal{K}^{(2)} + i\hbar g^2 \mathcal{A}_1^{(1)} |a_{1,s}|^2 \mu_+^{(2)*}} + ig \delta x_+^{(1)} \delta a_{1+}^{(1)}. \quad (31)$$

Here \mathcal{B} , in terms of $\delta x_+^{(1)}$ and $\delta a_{1+}^{(1)}$, can be taken as a constant. We see that in comparison with the linear process, the second-order sideband experiences a frequency shift $|\mathbf{Re}(C_2) - \mathbf{Re}(C_1)| \sim 10$ MHz, i.e., agreeing with our numerical results in the order of magnitudes.

4. Conclusions and Discussions

We theoretically investigate the impact of loss on OMIT in a passive compound COM system by coupling an external nanotip to the optical resonator. Loss-induced transparency is found at the EP in the OMIT transmission spectrum, which is reminiscent of that as reported in Ref. [56], but here corresponding to the off-resonance case (i.e., with $\Delta_P = \pm 3$ MHz). For the resonance case, however, increasing the tip loss leads to very minor changes for the OMIT peak. We also find that a slow-to-fast light switch can happen in the vicinity of the loss-induced EP. A detailed comparison between the linear OMIT process and its second-order sidebands, in the presence of a tunable tip loss, is also given, indicating that more exotic EP-assisted effects may happen in a nonlinear COM system. In practice, our work provides a promising new way to manipulate or switch both light transmissions and optical group delays with various COM devices. Finally, in view of the sensitive change of the optical group delay at the EP, our work also indicates a new way to achieve EP-enhanced sensing [61–63].

Funding

This work is supported by NSF of China under Grants No. 11474087 and No. 11774086, and the HuNU Program for Talented Youth.